01 Apr 2016

An Equivalent Circuit Model For Graphene-Based Terahertz Antenna Using The PEEC Method

Ying S. Cao

Li (Lijun) Jun Jiang
Missouri University of Science and Technology, ljf82@mst.edu

Albert E. Ruehli
Missouri University of Science and Technology, ruehlia@mst.edu

Recommended Citation

Y. S. Cao et al., "An Equivalent Circuit Model For Graphene-Based Terahertz Antenna Using The PEEC Method," *IEEE Transactions on Antennas and Propagation*, vol. 64, no. 4, pp. 1385 - 1393, article no. 7393520, Institute of Electrical and Electronics Engineers, Apr 2016.
The definitive version is available at https://doi.org/10.1109/TAP.2016.2521881

An Equivalent Circuit Model for Graphene-Based Terahertz Antenna Using the PEEC Method

Ying S. Cao, *Student Member, IEEE*, Li Jun Jiang, *Senior Member, IEEE*, and Albert E. Ruehli, *Life Fellow, IEEE*

***Abstract*—The electromagnetic (EM) characterization of graphene under general EM environments is becoming of interest in the engineering and scientific research fields. However, its numerical modeling process is extremely cost prohibitive due to the huge contrast between its thickness and other dimensions. In this work, for the first time, the EM features of graphene are characterized by a circuit model through the partial element equivalent circuit (PEEC) method. The atomically thick graphene is equivalently replaced by an impedance boundary condition. After incorporating the PEEC method, a novel surface conductivity circuit model is derived for graphene. A physical resistor and inductor are added into the conventional PEEC cell due to the dispersive conductivity property of graphene. The proposed novel method significantly reduces the memory and CPU time consumption for general graphene structures when compared with standard numerical finite element method (FEM) or finite difference (FD) methods, where 3-D meshing is unavoidable. This model also transforms the surface conductivity of graphene into a vivid circuit, and physical properties of the material can be conveniently obtained, such as radiation, scattering, and resistance properties, when compared with method of moments (MOM). In addition, the radiation and scattering calculation by MOM entail the cumbersome steps of defining a bounding surface and implementing a multidimensional integrand, while in PEEC, these complications are entirely bypassed by the concise vector–matrix–vector product (VMVP) formulas. To validate the introduced algorithm, various numerical examples are presented and compared with existing references.**

***Index Terms*—Graphene, impedance boundary condition, partial element equivalent circuit (PEEC) method, surface conductivity.**

I. Introduction

GRAPHENE, a flat monoatomic layer of carbon atoms distributed in a two-dimensional (2-D) layer, has recently attracted the attention of both academic and industry communities because of its unique mechanical, thermal, chemical, electronic, and optical characteristics [1]–[3]. Due to its novel characteristics, graphene has given rise to a plethora of potential applications, including graphene-based wireless communication, tunable nanopatch antenna [4], semiconductor, and surface plasmon waveguide. The surface conductivity of graphene denoted as $\sigma_g(\omega, \mu_c, \tau, T)$ plays a pivotal role in surface plasmon polariton (SPP), nanopatch antenna, and so on, where σ_g is a function of temperature T, chemical potential μ_c (dependent on carrier density, electrostatic bias, chemical doping), and relaxation time τ. By dynamically tuning the surface conductivity, the propagation, polarization, radiation, and scattering of electromagnetic (EM) waves through graphene can be manipulated.

The surface conductivity of graphene is composed of two parts: 1) intraband contribution σ_{intra}, and 2) interband contribution σ_{inter}. When the frequency is below the infrared range, the intraband dominates in the total conductivity. Otherwise, the interband σ_{inter} is predominant. To investigate the EM properties of graphene, various numerical methods have been developed such as the method of moments (MOM) [5], finite-difference time-domain (FDTD) method [6]. In general, two approaches can be applied when incorporating graphene into numerical methods. In the first, the graphene is considered as a 3-D thin layer with a finite thickness [7]. Hence, volumetric meshing is unavoidable. In this approach, the surface conductivity is transformed into an equivalent permittivity. In the second, the graphene is modeled as an infinitesimal resistive sheet in which the impedance boundary condition is satisfied. For this method, particularly, fine mesh structures are avoidable. It will not result in extremely stringent mesh size, which no doubt significantly decreases the memory load and CPU time.

The partial element equivalent circuit (PEEC) method proposed in the 1970s [8]–[10] is based on the electric field integral equation (EFIE) with potentials and currents as unknowns suitable for circuit models for EM problems. The approach turns the EM field solving into a circuit problem. A large category of PEEC applications is for EM compatibility (EMC), IC packaging, antenna characteristic analysis, and power calculation [11]. So far, nobody has ever tried to apply PEEC method into the graphene modeling.

In this work, the PEEC method is applied to convert the EM characterization of graphene into a circuit modeling process based on the impedance boundary condition. By analyzing the circuit model, graphene's EM properties can be predicted conveniently. For a graphene patch, the unit PEEC mesh model is applied, and the impedance boundary condition is transformed into a complex impedance, in which the real part corresponds to a physical resistor, and the imaginary part is a series of an inductor and a capacitor. By adding the physical resistor and

Manuscript received June 08, 2015; revised November 04, 2015; accepted January 10, 2016. Date of publication January 26, 2016; date of current version April 05, 2016. This work was supported in part by the Research Grants Council of Hong Kong (GRF 712612 and 711511), in part by NSFC 61271158, in part by HKU Seed Fund 201309160052, and in part by Hong Kong UGC AoE/P–04/08.

Y. S. Cao and L. J. Jiang are with the Department of Electrical and Electronic Engineering, University of Hong Kong, Hong Kong (e-mail: caoying@eee.hku.hk; jianglj@hku.hk).

A. E. Ruehli is with the UMRI/MST EMC Laboratory, Missouri University of Science and Technology, Rolla, MO 65409 USA (e-mail: albert.ruehli@gmail.com).

Color versions of one or more of the figures in this paper are available online at http://ieeexplore.ieee.org.

Digital Object Identifier 10.1109/TAP.2016.2521881

inductor into the conventional PEEC circuit unit cell, a novel PEEC model for graphene is proposed.

The advantage of the proposed new modeling process is: 1) when compared with the MOM [5], a circuit model of graphene under the EM environment is mathematically derived instead of physically predicted. It provides a reliable graphene modeling process that could be applied under complex environments. 2) The method is generally applicable to various shapes of graphene objects since the model is derived from the EFIE. 3) The proposed method is more efficient than the volumetric-based graphene modeling method such as finite difference (FD) [6] methods, since it does not need meshes along the thickness direction. Compared with the conventional impedance boundary condition-based methods, the proposed method is not a direct numerical approach. It provides the SPP frequency prediction purely based on the extracted circuit model instead of numerically resultant current distributions. 4) The proposed method has the potential to link the graphene EM modeling with lumped circuit components in practical applications, for instance, graphene antennas with nonlinear circuit components. 5) The definition of the absorption cross section (σ_{abs}), extinction cross section (σ_{ext}), and scattering cross section (σ_{sca}) are redefined based on the PEEC method, which is also the first time based on the authors' knowledge. By taking advantage of the newly defined PEEC model and the proposed cross sections, the resonant frequencies and other physical parameters are more transparent for people to calculate and understand.

This paper is organized as follows. Section II gives a brief introduction on the novel PEEC model for graphene, and Section III investigates several benchmarks to verify the proposed idea, including varying relaxation time τ, chemical potential μ_c, and adding substrates. Conclusion and discussions are presented at the end of this paper.

II. Theoretical Background

A. Extinction, Absorption, and Scattering Cross Section Calculated by PEEC

PEEC method is based on the EFIE. The total electric field is the superposition of incident field and the scattered field, which is

$$\begin{aligned}\mathbf{E}_{total} &= \mathbf{E}_{inc} + \mathbf{E}_{sca} \\ &= \mathbf{E}_{inc} - \frac{\partial \mathbf{A}}{\partial t} - \nabla\phi \\ &= \frac{\mathbf{J}}{\sigma}\end{aligned} \tag{1}$$

where $\mathbf{A}$ and ϕ are vector and scalar potentials, respectively.

According to the distributed power characterization by the PEEC method [11], the absorbed and scattered power can be represented by vector–matrix–vector product (VMVP) formulas without the cumbersome integration over a bounding surface, which are

$$P_{abs} = P^{ohm} \tag{2a}$$

$$P_{sca} = P^{r} \tag{2b}$$

where P^r and P^{ohm} are the radiated power and ohmic power loss. They can be conveniently represented and calculated by PEEC based on the new method in [11]. For instance, a typical EM structure may contain many components. After discretizing all the components for this structure, the radiated and ohmic power from the component labeled a are formulated as

$$P^{r'}_{a(a)} = \frac{1}{2}\mathrm{Re}\left(\mathbf{I}_a^{L\dagger}\overline{\mathbf{Z}}_L^{aa}\mathbf{I}_a^L + \mathbf{I}_a^{C\dagger}\overline{\mathbf{Z}}_C^{aa}\mathbf{I}_a^C\right) \tag{3a}$$

$$P^{ohm}_a = \frac{1}{2}\mathbf{I}_a^{L\dagger}\overline{\mathbf{Z}}_{ohm}^{aa}\mathbf{I}_a^L \tag{3b}$$

where the superscript "$\dagger$" means the conjugate transpose of a vector. $\mathbf{I}_a^L$ is the vector of current distribution of inductive branches on a. $\overline{\mathbf{Z}}_L^{aa}$ is an $N_{L_a} \times N_{L_a}$ matrix in which all elements are inductive coupling impedances (N_{L_a} is the number of inductive cells on a. $\overline{\mathbf{Z}}^{aa}_{L(mk)} = j\omega L p_{mk}$), and the $\overline{\mathbf{Z}}_C^{aa}$ is an $N_{C_a} \times N_{C_a}$ matrix whose elements correspond to capacitive coupling (N_{C_a} is the number of capacitive cells on a. $\overline{\mathbf{Z}}^{aa}_{C(mk)} = \frac{P_{p_{mk}}}{j\omega}$). $\overline{\mathbf{Z}}^{aa}_{ohm}$ is a diagonal matrix which contains the resistive part of each cell.

Based on the power analysis [11], the absorption, scattering, and extinction cross sections are reformulated as

$$\sigma_{abs} = \frac{P_{abs}}{|\mathbf{S}_{inc}|} \tag{4a}$$

$$\sigma_{sca} = \frac{P_{sca}}{|\mathbf{S}_{inc}|} \tag{4b}$$

$$\sigma_{ext} = \sigma_{abs} + \sigma_{sca}. \tag{4c}$$

Equations (3) and (4) convert the calculation process for cross sections into an intrinsic circuit problem that can be solved without involving direct electric and magnetic field calculations.

B. PEEC Model of a Graphene Patch

According to the PEEC scheme, a general graphene patch is composed of many PEEC cells. Each cell can be rectangular, triangular, or general convex polygons. The rectangular shape is the most convenient unit cell structure for PEEC because a lot of analytical solutions exist for the equivalent component calculations. PEEC algorithms based on rectangles can also be extended to other polygon shapes. For convenience, this paper focuses on rectangular PEEC cells only.

For each rectangular PEEC cell, a unit equivalent circuit can be derived from EFIE in (1). Each unit equivalent circuit contains R, L, and C components. Based on the surface conductivity of graphene, which is introduced in Appendix, the impedance part is directly determined by the surface conductivity. The analogy between a graphene complex conductivity model and a series circuit is shown in Fig. 1. σ here is the total surface conductivity of graphene with both intraband and interband contributions, which is studied in detail in Appendix A. Considering a one-cell PEEC model for a free-standing rectangular patch with the length l and width w, the surface resistance of the patch is formulated as

$$\begin{aligned}R_{surf} &= \frac{l}{w\sigma(\omega)} \\ &= R_r + j\omega L_r + Z_{inter}\end{aligned} \tag{5}$$

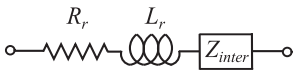

Fig. 1. Analogy between circuit elements and complex conductivity of graphene, in which R_r and L_r are due to intraband contribution while Z_{inter} is for interband impedance.

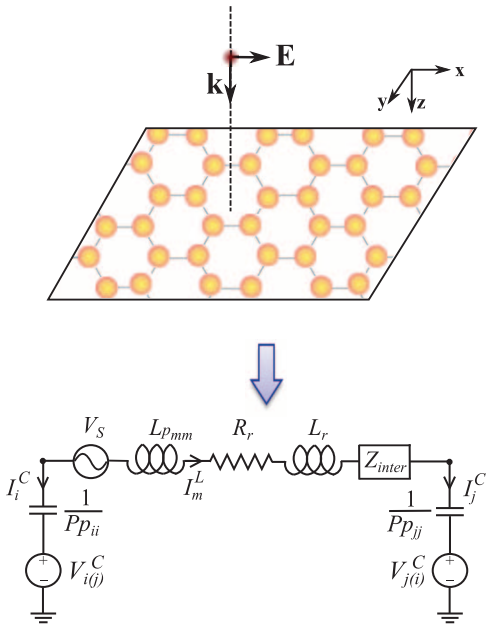

Fig. 2. One PEEC cell model for a graphene patch, in which R_r, L_r, and Z_{inter} are from surface conductivity, and they are formulated as (5). V_s is the voltage source due to external electric field. Lp_{mm}, Pp_{ii}, and Pp_{jj} are self-inductance and self-coefficients of potential for PEEC model, respectively. $V_{i(j)}^C$ and $V_{j(i)}^C$ are the VCVSs due to mutual capacitive coupling between two capacitors i and j.

where $\sigma(\omega)$ is introduced in detail in Appendix, R_{surf} means total surface impedance from graphene's conductivity, R_r and L_r denote resistance and inductance from the intraband part, respectively. Z_{inter} is the impedance from the interband contribution. When the frequency is relatively low, the intraband contribution dominates the total surface conductivity.

For graphene, its conductivity is complex and dispersive. To build a PEEC model compatible to graphene, we can analogize the real part of conductivity represents loss of graphene as the resistive effect of the circuit in Fig. 1, whereas the imaginary part of graphene's conductivity is related to the stored energy similar to the inductive or capacitive effect in the circuit model. Z_{inter} is a complex impedance which corresponds to the interband contribution on surface conductivity. According to [16], the imaginary part of graphene's conductivity can attain positive or negative values. Hence, we can identify the reactive response of the derived equivalent circuit components through the sign of its imaginary part.

Based on (5), a representative-derived PEEC cell circuit model for one graphene patch is illustrated in Fig. 2 by applying voltage control voltage sources (VCVSs). Other type sources such as current control current sources (CCCSs) in capacitive branches can also be proposed according to [17] and [18].

For simplicity, if the frequency is relatively low, the intraband contribution dominates (as Fig. 5 depicts). Hence, the interband contribution for surface conductivity is neglected. For a one-cell PEEC model of a free standing rectangular patch with the length l and width w, the surface resistance of the patch is formulated as

$$R_{surf} = \frac{l}{w\sigma_{intra}(\omega)} = R_r + \mathrm{j}\omega L_r \tag{6}$$

where σ_{intra} is the intraband contribution for the surface conductivity, as seen in Appendix. R_{surf} is split into two parts: a real part and an imaginary part. The real part corresponds to a physical resistor R_r. The imaginary part is proportional to ω, which physically means a pure inductor L_r. Each component in (6) can be rewritten as

$$R_r = \frac{l}{w}\frac{\tau^{-1}}{\frac{2e^2k_BT}{\pi\hbar^2}\ln\left[2\cosh\left(\frac{\mu_c}{2k_BT}\right)\right]} \tag{7a}$$

$$L_r = \frac{l}{w}\frac{1}{\frac{2e^2k_BT}{\pi\hbar^2}\ln\left[2\cosh\left(\frac{\mu_c}{2k_BT}\right)\right]} \tag{7b}$$

in which R_r corresponds to the ohmic loss in this conducting material. From (7b), one can see that if only the intraband contribution of the surface conductivity is considered, the reactance part of (6) is always positive.

C. Resonant Frequency Calculation Based on the PEEC Model

The proposed graphene equivalent circuit model provides two novel approaches to predict resonant frequencies.

1) Numerical Approach Based on PEEC Circuit Model: For one rectangular graphene patch modeled by the unit circuit cell in Fig. 2, the absorption cross section σ_{abs} is proportional to I_m^{L2} based on (2a). By solving the circuit model, it can be found that the absolute values of the branch current I_m^L reach maximums at certain frequency points. They correspond to the resonant frequencies. For a general graphene structure, it is composed of many PEEC unit cells similar to that in Fig. 2, and these cells couple with each other. By applying the modified nodal analysis (MNA) [12] to obtain the overall current distributions, it is easy to figure out the resonance locations and their resonant frequencies on the graphene. This process is similar to [5], but it does not need the MOM process. It utilizes the common SPICE solver [13] which can be done in both time domain and spectral domain.

One example is given for a x-direction free-standing $5 \times 0.5\ \mu\mathrm{m}^2$ graphene strip with a vertically incident x-direction polarized plain wave. It is analyzed by the proposed PEEC model and the current distribution along the patch length is illustrated in Fig. 3. It can be concluded that when the frequency reaches the resonant point, the x-direction current distribution on the patch shows strong standing wave patterns and noticeable current enhancements can be observed on the patch. Hence, the proposed graphene circuit model can be conveniently analyzed using existing circuit solvers without writing new numerical engines to predict the physical characteristics of the graphene patch.

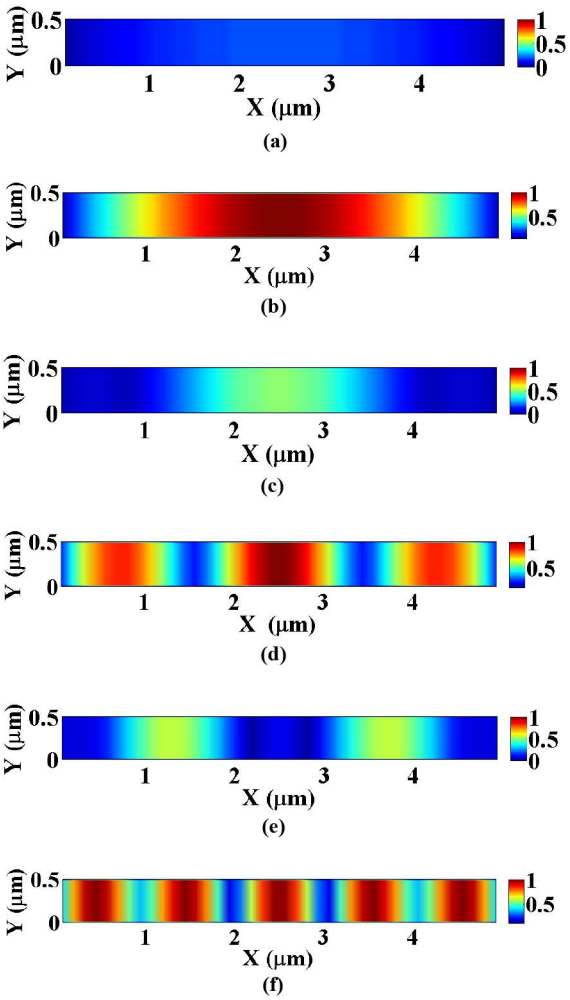

Fig. 3. Current distribution in x-direction on the geometry of the 5×0.5 μm^2 patch ($T = 300$ K, $\tau = 10^{-12}$ s). (a) $f = 0.50$ THz (below the first resonant frequency point). (b) $f = 0.95$ THz which is the first resonant frequency. Noticeable current enhancement is observed at this frequency. (c) $f = 2.00$ THz (between the first and second resonant frequency). (d) $f = 2.24$ THz which is the second resonant frequency. (e) $f = 3.00$ THz (between the second and third resonant frequency). (f) $f = 3.30$ THz which is the third resonant frequency.

2) Analytical Approach Based on the PEEC Circuit Model: Based on the proposed PEEC model, the spontaneous plasmon polariton resonance frequency can be computed directely from the resultant equivalent circuit. Fig. 4 shows the partial equivalent circuit of four current filaments sharing the same common node in the PEEC partition on the graphene patch. Each branch is a simplification of the circuit given in Fig. 2. Several simplifications are taken in construction of the circuit in Fig. 4. First, the impedance from the interband contribution in the conductivity is ignored because the working frequency is focused in the THz range. Second, because the SPP is due to the local collective resonance, the coupling between branches is ignored. Hence, voltage control sources and mutual partial inductances are not involved in the model. Third, a uniform mesh along all orthogonal directions is assumed. Hence, a factor 1/2 is introduced to every component around the shared node to maximize the simplification of the model. For a 2-D CRLH TL model,

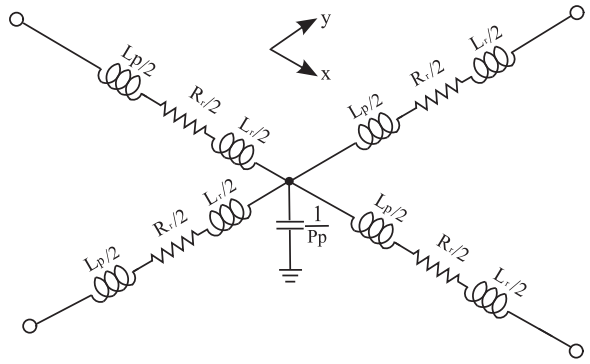

Fig. 4. Unit model for uniform PEEC cell of graphene. This model has slight differences with 2-D CRLH model [19] since free-space graphene does not take ground plane coupling into account whereas the each fundamantal loop in a PEEC model has capacitances to ground.

there shall be a coefficient 1/2 to represent the unit circuit cell, since this cell will combine with nearby cells in both directions (for Fig. 4 they are x- and y-directions) with the same inductances and resistances.

This proposed model is very similar to a classic transmission line (TL) model, especially those in composite right- and left-handed (CRLH) TL models [19]. However, there are fundamental differences between the proposed model and the TL model. The graphene structure considered in this paper can consist of a single or multiple sheets. Each sheet can be modeled separately. It is shown that TL models can be used to represent the behavior of graphene structures using the circuit elements per unit length computed for the PEEC model. Based on the assumption, the branch impedance $Z'(\omega)$ and shunt admittance $Y'(\omega)$ are

$$\begin{aligned} Z'(\omega) &= R_r' + j\omega L_r{}' + j\omega Lp' \\ &= R_r' + j\omega L' \qquad (8a) \\ Y'(\omega) &= j\omega C' \qquad (8b) \end{aligned}$$

where $R = R_r,\ C = 1/Pp,\ L = Lp + L_r,\ L' = L/p,\ R' = R/p$, and $C' = C/p$. Lp and Pp are partial inductance and partial coefficient of potential, respectively. L' is the summation of L_r' and Lp', p is the length of one unit cell, and the superscript means that the R, L, and C components are divided by the unit length p. They are per-unit length resistance, inductance, and capacitances, respectively.

Further, we have a propagation constant in each branch defined as

$$\gamma = \alpha + j\beta = \sqrt{Z'Y'}. \qquad (9)$$

Hence, the dispersion relationship for graphene can be derived to be

$$\omega^2 = \frac{(\beta p)^4}{LC(\beta p)^2 + R^2C^2/4}. \qquad (10)$$

It is interesting to see that if $R = 0$ in the above equation, this equation reduces to a conventional right-handed TL model dispersion relation $\beta p = \omega\sqrt{LC}$.

According to the condition for Fabry–Pérot-type resonator

$$l_{eff} = m\frac{\pi}{\beta} \tag{11}$$

where m is an integer and l_{eff} is the effective resonator length.

For a simpler case, letting $R = 0$ (lossless case) in (10), (10) and (11) result in

$$\omega = \frac{mp}{l_{eff}}\frac{\pi}{\sqrt{LC}}. \tag{12}$$

By solving (12), the frequencies for the first, second, and third resonant points can be calculated.

If $R \neq 0$, (11) becomes $\beta p = m\pi p/l_{eff}$. Combining this equation with (10), we have

$$\omega^2 = \frac{(m\pi/N)^4}{LC(m\pi/N)^2 + R^2C^2/4} \tag{13}$$

where $N = l_{eff}/p$. Regarding to the fact that p is the length of a unit cell, and l_{eff} is the effective resonator length, N can be set to 10, 20, or bigger if needed. One thing to be noted is that p/λ is smaller than 1/20 to ensure the accuracy of this model. Hence, N shall be larger than $20\times l_{eff}/\lambda$.

Given a PEEC cell of graphene patch (relaxation time $\tau = 10^{-12}$ s, $\mu_c = 0$ eV), we have $N = 10$, $L = 10^{-9}$ H, $Pp = 5 \times 10^{17}$ F^{-1}, and $R = 10^3$ Ω. Taking these parameters into (13), we have the first resonant frequency as

$$f^1_{estm} = 1.12 \text{ THz} \tag{14}$$

where f^1_{estm} means the estimated first resonant frequency according to this analytical approach. This frequency matches those in Fig. 7 very well, which states that the first resonant frequency of a 5×0.5 μm^2 patch with $\tau = 10^{-12}$ s and $\mu_c = 0$ eV is around 1 THz.

Theoretically, higher order resonant frequencies can also be calculated according to (12), which means that m can be 2, 3 or higher values. For the same example, we can get

$$f^2_{estm} = 2.24 \text{ THz} \tag{15a}$$

$$f^3_{estm} = 3.36 \text{ THz} \tag{15b}$$

where f^2_{estm} and f^3_{estm} are the estimated second and third resonant frequencies, respectively. The predicted resonant points by (12) match very well with the full-wave simulated results by PEEC which is illustrated in Fig. 7. These results agree well with the current distributions depicted in Fig. 3, which indicates that this PEEC-based analytical model behaves well in the SPP approximation.

III. Numerical Results

In this section, various numerical examples are introduced to verify and validate the proposed algorithm by studying the cross sections of a graphene sheet.

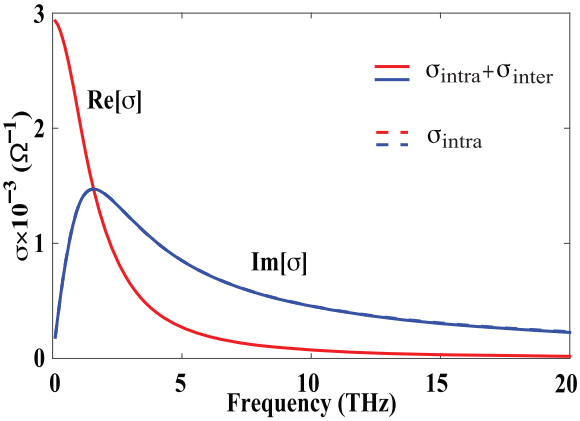

Fig. 5. Real and imaginary parts of the surface conductivity corresponding to different frequencies at room temperature (T = 300 K), relaxation time $t = 10^{-13}$ s, and zero electrostatic bias ($\mu_c = 0.25$ eV). The solid lines are surface conductivity with both intraband and interband contributions, while the dashed lines are for the intraband contribution only.

A. Surface Conductivity of an Infinitely Large Graphene Sheet

Graphene's complex conductivity ($\sigma = \sigma_r$-jσ_i, where σ_r and σ_i are the real and imaginary parts of the surface conductivity, respectively) depends on the radian frequency ω, relaxation time τ representing the loss mechanism, temperature T, and chemical potential μ_c.

The surface conductivity changes with frequency as (16)–(19) show in Appendix, as is illustrated in Fig. 5.

Fig. 5 shows that within this frequency range (below 20 THz), the intraband contribution plays a vital role in the total conductivity. However, in this paper, both intraband and interband contributions are taken into account in order to maintain a high numerical accuracy.

B. A Microsize Graphene Patch

To validate the proposed algorithm for graphene, a 5×10 μm^2 freestanding patch in [4] is visited. The parameters of surface conductivity are $T = 300$ K, $\mu_c = 0$ eV, and $\tau = 10^{-13}$ s. The graphene patch is illuminated by a plane wave linearly polarized along the patch length. The excitation process is shown in Fig. 10.

Fig. 6 illustrates that the proposed method reaches a very good agreement with [4].

C. Relaxation Time

The relaxation time of a material is the time that it takes for a charge distortion as fluctuation to relax to a uniform charge density after it has been introduced in the material. The relaxation time in graphene depends on the quality of the graphene sample, and it is a fundamental parameter of its conductivity model. We consider a graphenna composed of a graphene patch with a size of 5×0.5 μm^2. Since no common agreement exists for the value of the relaxation time in graphene, we consider its influence on the radiation properties of graphene antennas.

The absorption cross section of the graphene patch is shown in Fig. 7 for different relaxation times. It is clearly seen that

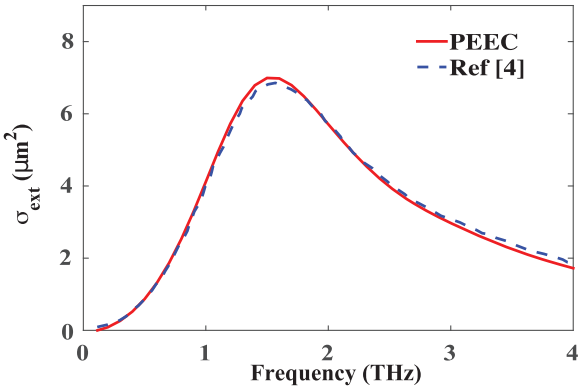

Fig. 6. Extinction cross section of a graphenna as a function of frequency with different methods: PEEC (red line) and [4] (blue-dashed line).

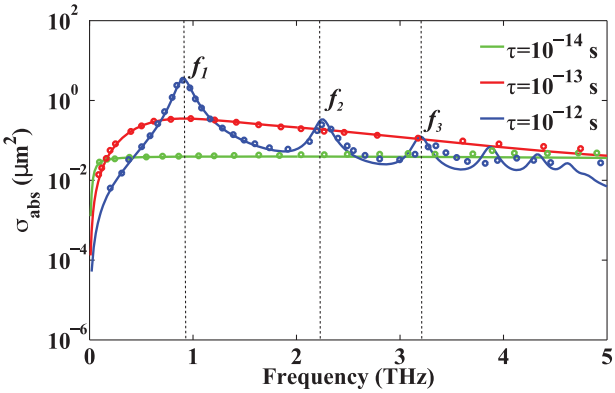

Fig. 7. Absorption cross section (in logarithmic scale) of a graphene patch as a function of frequency, for different relaxation times: 10^{-14} (green line), 10^{-13} (red line), and 10^{-12} (blue line). The results are compared with [20] different relaxation times: 10^{-14} (green circles), 10^{-13} (red circles), and 10^{-12} (blue circles), in which f_1, f_2, and f_3 are resonant frequencies when $\tau = 10^{-12}$ s, and $f_1 = 0.95$ THz, $f_2 = 2.24$ THz, and $f_3 = 3.30$ THz. Current distributions in these frequency points are illustrated in Fig. 3.

the chosen value for the relaxation time has a huge impact on the resonant character of the graphenna and its bandwidth. In particular, for $\tau = 10^{-14}$ s, the resonant phenomenon does not occur for the graphene antenna withnin this frequency range. When $\tau = 10^{-13}$ s, a wide resonant around 0.95 THz is observed, with a -3 dB bandwidth of 1.9 THz. As the relaxation time continues to increase, higher order resonances appear, and a more intense resonant behavior is observed. Furthermore, the $-3-$dB bandwidth diminishes dramatically, to 0.16 THz in the case of $\tau = 10^{-12}$ s.

Given that the main application envisaged for graphennas consists of wireless communications among nanosystems, a bandwidth as large as possible is desired in order to maximize the channel capacity. Therefore, we conclude that the optimal value of the relaxation time for graphennas is around $\tau = 10^{-13}$ s, in order to achieve a resonant behavior while maintaining a radiating bandwidth as large as possible.

D. Chemical Potential

The chemical potential will affect the surface conductivity, and the amount of power absorbed by the graphene patch,

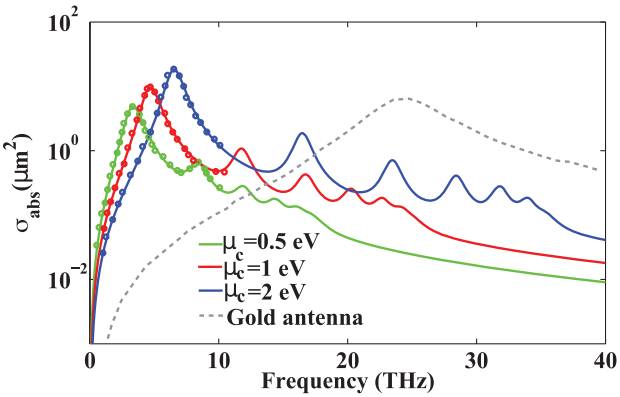

Fig. 8. Absorption cross section (in logarithmic scale) of a graphene patch as a function of frequency, for different values of chemical potential: 0.5 (green line), 1 (red line), and 2 eV (blue line), which are compared with [20]: 0.5 (green circles), 1 (red circles), and 2 eV (blue circles). The results are compared with an equivalent gold antenna with the same size (gray-dashed line).

TABLE I
RESONANT FREQUENCY OF A GRAPHENE PATCH WITH LENGTH 5 μM AND WIDTH 0.5 μM AS A FUNCTION OF THE CHEMICAL POTENTIAL

Chemical potential (eV)	Resonant frequency (THz)	
	[20]	PEEC
0	0.918	0.92
0.5	3.356	3.35
1	4.704	4.70
2	6.541	6.55

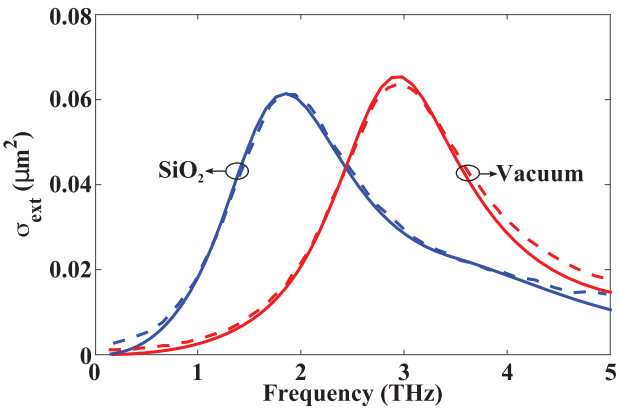

Fig. 9. Extinction cross section of a graphene patch as a function of frequency, for different values of dielectric constant: silica ($\epsilon = 4.0$, blue line) and vacuum (red line), which are compared with [4]: silica (blue-dashed line) and vacuum (red-dashed line).

and, in consequence, its resonant frequency. The absorption cross sections corresponding to different frequencies of the 5×0.5 μm^2 patch are shown in Fig. 8.

Indeed, as can be observed, the maximum absorption cross section increases dramatically as the chemical potential changes from 0.5 to 2 eV. Furthermore, as shown in Table I, the resonant frequency of the graphene antenna also changes dramatically when varying the chemical potential. However, the resonant frequency remains below that of a metallic antenna with the same size.

E. Dielectric Substrate

The dielectric substrate influences both the spectral position and magnitude of the resonance. In Fig. 9, the extinction cross section of the graphene antenna with length $L = 1$ μm and width $W = 0.5$ μm supported by different infinite substrates is shown. With the increase of dielectric constant, resonant frequency decreases significantly.

For finite substrate cases, the multilayer Green's function [21] can be incorporated into the PEEC formulation. Hence, other results of interest can be obtained [22].

IV. Conclusion

In this paper, a novel circuit model is derived for the graphene sheet based on the PEEC algorithm in the THz frequency band. Instead of using volumetric meshes for the atomically thick graphene, the impedance boundary condition is applied with the surface conductivity σ_g gauged by the Kubo-formula. The equivalent circuit is derived using the complex conductivity and the geometrical PEEC mesh. The EM features of graphene in the EM field can be obtained by solving the resultant circuit model inside the circuit solver. The SPP resonant frequencies can be obtained from circuit components directly. The validation and applicability of the proposed algorithms are demonstrated by several numerical examples.

Appendix A
Theoretical Background

A. Surface Conductivity of Graphene

The surface conductivity of an infinite graphene film can be calculated by the means of the Kubo formula. It has been experimently demonstrated [23] that the edge effects of the graphene conductivity only appear in structures with graphene lateral size smaller than 100 nm. Hence, in this paper, the edge effects are not considered here. By the random-phase approximation, the surface conductivity can be represented as a local form with the Drude-like intraband contribution [20]

$$\sigma_{intra}(\omega) = \frac{2e^2}{\pi\hbar}\frac{k_B T}{\hbar}\ln\left[2\cosh\left[\frac{\mu_c}{2k_B T}\right]\right]\frac{-\mathrm{j}}{\omega - \mathrm{j}\tau^{-1}} \quad (16)$$

and the interband contribution given by [20]

$$\sigma_{inter}(\omega) = \frac{e^2}{4\hbar}\left(H\left(\frac{\omega}{2}\right) - \mathrm{j}\frac{4\omega}{\pi}\int_0^\infty d\varepsilon \frac{H(\varepsilon) - H(\omega/2)}{\omega^2 - 4\varepsilon^2}\right). \quad (17)$$

Here, τ is the relaxation time, T is the temperature, μ_c is the chemical potential, and $H(\varepsilon)$ is defined as

$$H(\varepsilon) = \frac{\sinh(\hbar\varepsilon/k_B T)}{\cosh(\mu_c/k_B T) + \cosh(\hbar\varepsilon/k_B T)}. \quad (18)$$

The total conductivity is the summation of contribution from both intraband and interband. Hence

$$\sigma(\omega) = \sigma_{intra}(\omega) + \sigma_{inter}(\omega). \quad (19)$$

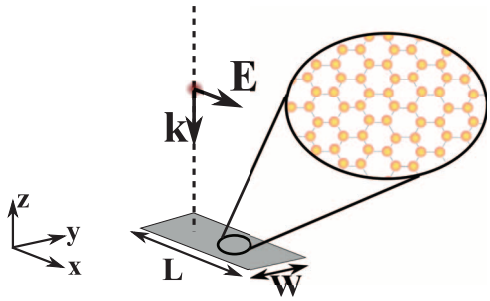

Fig. 10. Sketch of a graphene film placed in air with length L and width W.

When the frequency is relatively low, the intraband contribution will be dominant. While for very high frequencies, the interband contribution will dominate the total conductivity.

The graphene patch is placed in air, and a plane wave is linearly polarized along the length of the patch, which is illustrated in Fig. 10.

The surface conductivity connects the tangential electric field and the surface electric current. The impedance boundary condition at $z = 0$ can be represented as

$$\hat{\mathbf{n}} \times (\mathbf{H}_{|z=0^+} - \mathbf{H}_{|z=0^+}) = \mathbf{J}_{surf} = \sigma(\omega)\mathbf{E} \quad (20)$$

where the boundary condition is for the graphene patch only. $\mathbf{J}_{surf}$ is the surface current density on the graphene patch, and $\sigma(\omega)$ is the surface conductivity of graphene.

B. Extinction, Absorption, and Scattering Power Calculation

The extinction power is the total power removed from the incident field (the sum of the absorbed and the scattered powers) due to the presence of the scattering object Ω. The absorbed power is the power flowing into the body and the power scattered from an object Ω is given by the real part of the integral of the outward-directed normal component of $\mathbf{S}_{sca}$ over $\partial\Omega$. $\mathbf{S}_{tot}$ is the time average Poynting vector. $\mathbf{S}_{inc}$, $\mathbf{S}_{sca}$, and $\mathbf{S}_{ext}$ are incident, scattered, and extinguished components of the Poynting vector. According to [15], $P_{ext} = P_{sca} + P_{abs}$, in which

$$P_{abs} = \oiint_{\partial\Omega} \langle \mathbf{S}_{tot} \rangle \cdot \hat{\mathbf{n}} \quad (21a)$$

$$P_{sca} = \oiint_{\partial\Omega} \langle \mathbf{S}_{sca} \rangle \cdot \hat{\mathbf{n}}. \quad (21b)$$

It is interesting to decompose the time-average Poynting vector

$$\langle \mathbf{S}_{tot} \rangle \triangleq \frac{1}{2}\,\mathrm{Re}\left\langle \mathbf{E}_{tot} \times \bar{\mathbf{H}}_{tot} \right\rangle \quad (22)$$

in terms of incident, scattered, and extinguished components, where the common time-harmonic factor $\exp(\mathrm{j}\omega t)$ (ω is the angular frequency and t is time) is omitted for the sake of brevity

$$\langle \mathbf{S}_{tot} \rangle = \langle \mathbf{S}_{inc} \rangle + \langle \mathbf{S}_{sca} \rangle + \langle \mathbf{S}_{ext} \rangle \quad (23)$$

where

$$\langle \mathbf{S}_{inc} \rangle \triangleq \frac{1}{2} \operatorname{Re} \left\langle \mathbf{E}_{inc} \times \bar{\mathbf{H}}_{inc} \right\rangle \tag{24a}$$

$$\langle \mathbf{S}_{sca} \rangle \triangleq \frac{1}{2} \operatorname{Re} \left\langle \mathbf{E}_{sca} \times \bar{\mathbf{H}}_{sca} \right\rangle \tag{24b}$$

$$\langle \mathbf{S}_{ext} \rangle \triangleq \frac{1}{2} \operatorname{Re} \left\langle \mathbf{E}_{sca} \times \bar{\mathbf{H}}_{inc} + \mathbf{E}_{inc} \times \bar{\mathbf{H}}_{sca} \right\rangle . \tag{24c}$$

REFERENCES

[1] A. Geim and K. Novoselov, "The rise of graphene," *Nat. Mater.*, vol. 6, no. 3, pp. 183–191, 2007.

[2] A. Castronero, F. Guinea, N. Peres, K. Novoselov, and A. Geim, "The electronic properties of graphene," *Rev. Mod. Phys.*, vol. 81, no. 1, pp. 109–162, 2009.

[3] Y. H. Wu, T. Yu, and Z. X. Shen, "Two-dimensional carbon nanostructures: Fundamental properties, synthesis, characterization, and potential applications," *J. Appl. Phys.*, vol. 108, p. 071301, 2010.

[4] I. Llsater, C. Kremers, A.-C. Aparicio, J. M. Jornet, E. Alarcon, and D. N. Chigrin, "Graphene-based nano-patch antenna for terahertz radiation," *Photon. Nanostruct. Fundam. Appl.*, vol. 10, pp. 353–358, May 2012.

[5] O. V. Shapoval, J. S.-G. Diaz, J.-P. Carrier, J. R. Mosig, and A. I. Nosich, "Integral equation analysis of plane wave scattering by coplanar graphene strip gratings in the THz range," *IEEE Trans. Terahertz Sci. Techn.*, vol. 6, no. 3, pp. 666–674, Sep. 2013.

[6] V. Nayyeri, M. Soleimani, and M. Ramahi, "Wideband modeling of graphene using the finite-difference time-domain method," *IEEE Trans. Antenna Propag.*, vol. 6, no. 12, pp. 6107–6114, Dec. 2013.

[7] I. Ahmed, E. H. Khoo, and E. Li, "Efficient modeling and simulation of graphene devices with the LOD-FDTD method," *IEEE Microw. Wireless Compon. Lett.*, vol. 23, no. 6, pp. 306–308, Jun. 2013.

[8] A. E. Ruehli, "Equivalent circuit models for three dimensional multiconductor systems," *IEEE Trans. Microw. Theory Techn.*, vol. MTT-22, no. 3, pp. 216–221, Mar. 1974.

[9] A. E. Ruehli, "Inductance calculations in a complex integrated circuit environment," *IBM J. Res. Develop.*, vol. 16, no. 5, pp. 470–481, Sep. 1972.

[10] A. E. Ruehli and P. A. Brennan, "Efficient capacitance calculations for three-dimensional multiconductor systems," *IEEE Trans. Microw. Theory Techn.*, vol. MTT-21, no. 2, pp. 76–82, Feb. 1973.

[11] Y. S. Cao, L. J. Jiang, and A. E. Ruehli, "Distributive radiation and transfer characterization based on the PEEC method," *IEEE Trans. Electromagn. Compat.*, vol. 57, no. 4, pp. 734–742, Aug. 2015.

[12] C. W. Ho, A. E. Ruehli, and P. A. Brennan, "The modified nodal approach to network analysis," *IEEE Trans. Circuits Syst.*, vol. CAS-22, no. 6, pp. 504–509, Jun. 1975.

[13] L. W. Nagel and D. O. Pederson, "Simulation program with integrated circuit emphasis (SPICE)," Memorandum No. ERL–M382, University of California, Berkeley, CA, USA, Apr. 1973.

[14] I. Llatser *et al.*, "Characterization of graphene-based nano-antennas in the terahertz band," in *Proc. 6th Eur. Conf. Antennas Propag. (EUCAP)*, Mar. 2012, pp. 194–198.

[15] C. F. Bohren and D. R. Huffman, *Absorption and Scattering of Light by Small Particles*. New York, NY, USA: Wiley-Interscience, 1983.

[16] A. Vakil and N. Engheta, "Transformation optics using graphene," *Science*, vol. 332, no. 6035, pp. 1291–1294, 2011.

[17] A. E. Ruehli, J. Garrett, and C. R. Paul, "Circuit models for 3-D structures with incident fields," in *Proc. IEEE Int. Symp. Electromagn. Compat.*, Dallas, TX, USA, Aug. 1993, pp. 28–31.

[18] A. E. Ruehli, G. Antonini, J. Esch, J. Ekman, A. Mayo, and A. Orlandi, "Nonorthogonal PEEC formulation for time and frequency-domain EM and circuit modeling," *IEEE Trans. Electromagn. Compat.*, vol. 45, no. 2, pp. 167–176, May 2003.

[19] A. Lai, C. Caloz, and T. Itoh, "Composite right/left-handed transmission line metamaterials," *IEEE Micro*, vol. 5, no. 3, pp. 34–50, Sep. 2004.

[20] I. Llatser *et al.*, "Radiation characteristics of tunable graphennas in the terahertz band," *Radioengineering*, vol. 21, no. 4, pp. 946–953, 2012.

[21] K. A. Michalski and J. R. Mosig, "Multilayered media Green's functions in integral equation formulations," *IEEE Trans. Antenna Propag.*, vol. 45, no. 3, pp. 508–519, Mar. 1997.

[22] Y. P. Chen, W. Sha, and L. J. Jiang, "Graphene plasmonics for tuning photon decay rate near metallic split-ring resonator in a multilayered substrate," *Opt. Exp.*, vol. 23, no. 3, pp. 2798–2807, Feb. 2015.

[23] M. Y. Han, B. Oezyilmaz, Y. Zhang, and P. Kim, "Energy band gap engineering of graphene nanoribbons," *Phys. Rev. Lett.*, vol. 98, p. 206805, 2007.

Ying S. Cao (S'14) received the B.S. degree in physics from the University of Science and Technology of China (USTC), Hefei, China, in 2012. Currently, she is pursuing the Ph.D. degree at the University of Hong Kong, Hong Kong.

In 2011, she was a Visiting Student studying and researching quantum teleportation with Clarendon Laboratory, University of Oxford, Oxford, U.K. Since 2012, she has been with the Center of Electromagnetics and Optics, University of Hong Kong. She has been a Visiting Scholar at the EMC Laboratory, Missouri University of Science and Technology, Rolla, MO, USA. Her research interests include computational electromagnetics, EMC/EMI, and multiphysics modeling.

Ms. Cao was the recipient of the Excellent Graduate Award of USTC in 2012.

Li Jun Jiang (S'01–M'04–SM'13) received the B.S. degree in electrical engineering from the Beijing University of Aeronautics and Astronautics, Beijing, China, in 1993, the M.S. degree from the Tsinghua University, Beijing, China, in 1996, and the Ph.D. degree from the University of Illinois at Urbana-Champaign, Champaign, IL, USA, in 2004

From 1996 to 1999, he was an Application Engineer with the Hewlett-Packard Company. Since 2004, he has been a Postdoctoral Researcher, a Research Staff Member, and a Senior Engineer with the IBM T.J. Watson Research Center, Yorktown Heights, New York, NY, USA. Since the end of 2009, he was an Associate Professor with the Department of Electrical and Electronic Engineering, the University of Hong Kong, Hong Kong. From September 2014 to March 2015, he was a Visiting Scholar with the University of California, Los Angeles, CA, USA. His research interests include electromagnetics, computational electromagnetics, IC signal/power integrity, IC EMC/EMI, antennas, multi-physics modeling, etc.

Dr. Jiang is an Associate Editor of IEEE TRANSACTIONS ON ANTENNAS AND PROPAGATION, an Editor of *Progress in Electromagnetics Research*, an Associate Guest Editor of the *Proceedings of IEEE* Special Issue in 2011–2012, an IEEE AP-S Member, an IEEE MTT-S member, an ACES member, and a member of Chinese Computational Electromagnetics Society. He was the Semiconductor Research Cooperation (SRC) Industrial Liaison for several academic projects. He was a TPC member of IEEE Electrical Design for Advanced Packaging and Systems (EDAPS) since 2010, a TPC member of 2013 IEEE International Conference on Microwave Technology and Computational Electromagnetics (ICMTCE), a Scientific Committee Member of 2010 Workshop on Simulation and Modeling of Emerging Electronics (SMEE), a special session organizer of IEEE EDAPS, the *International Review of Progress in Applied Computational Electromagnetics* (ACES), Asia-Pacific Radio Science Conference (AP-RASC), a co-organizer of HKU Computational Science and Engineering Workshops in 2010–2012, the TC-9 and TC-10 member of IEEE EMC-S since 2011, a TPC Chair of the 7th International Conference on Nanophotonics (ICNP), a TPC member of the 3rd Conference on Advances in Optoelectronics and Micro/Nano Optics (AOM), a Co-Chair of International Workshop on Pulsed Electromagnetic Field, Delft, The Netherlands, 2013, the Chair of the 14th IEEE Hong Kong AP/MTT Postgraduate Conference, and Session Chair of many international conferences. He also serves as a Reviewer of IEEE TRANSACTIONS on several topics, and other primary electromagnetics and microwave related journals. He was the recipient of the HP STAR Award, in 1998, the IEEE MTT Graduate Fellowship Award, in 2003, the Y.T. Lo Outstanding Research Award, in 2004, and the IBM Research Technical Achievement Award, in 2008.

Albert E. Ruehli (LF'03) received the Ph.D. degree in electrical engineering from the University of Vermont, Burlington, VT, USA, in 1972, and an honorary doctorate from the Lulea University, Luleå, Sweden, in 2007.

He has been a member of various projects with IBM including mathematical analysis, semiconductor circuits and devices modeling, and as Manager of a VLSI design and CAD Group. Since 1972, he has been with IBM's T.J. Watson Research Center, Yorktown Heights, New York, NY, USA, where he was a Research Staff Member with the Electromagnetic Analysis Group. He has been an Emeritus of IBM Research and an Adjunct Professor in the EMC area at the Missouri University of Science and Technology, Rolla, MO, USA. He is the Editor of two books, *Circuit Analysis, Simulation and Design* (North-Holland, 1986, 1987) and has authored/coauthored over 200 technical papers.

Dr. Ruehli has served in numerous capacities for the IEEE. In 1984 and 1985, he was the Technical and General Chairman, respectively, of the ICCD International Conference. He has been a member of the IEEE ADCOM for the Circuit and System Society and an Associate Editor for the IEEE TRANSACTIONS ON COMPUTER-AIDED DESIGN. He is a member of SIAM. He has given talks at universities including keynote addresses and tutorials at conferences, and has organized many sessions. He was the recipient of the IBM Research Division or IBM Outstanding Contribution Awards in 1975, 1978, 1982, 1995, and 2000, the Guillemin-Cauer Prize Award for his work on waveform relaxation, in 1982, and a Golden Jubilee Medal, in 1999, both from the IEEE CAS Society, a Certificate of Achievement from the IEEE EMC Society for inductance concepts and the Partial Element Equivalent Circuit (PEEC) method, in 2001, the 2005 Richard R Stoddart Award, the Honorary Life Member Award from the IEEE Electromagnetic Compatibility Society for "Outstanding Technical Performance," in 2007, and a Best Paper Award at the EPEPS conference for his work on optimized waveform relaxation, in 2010.